

 Open access • Journal Article • DOI:10.1126/SCIENCE.AAN0202

Two-dimensional sp² carbon–conjugated covalent organic frameworks

— [Source link](#) 

Enquan Jin, Mizue Asada, Qing Xu, Sasanka Dalapati ...+7 more authors





Institutions: Japan Advanced Institute of Science and Technology, Nottingham Trent University, Lawrence Berkeley National Laboratory, Leipzig University

Published on: 18 Aug 2017 - Science (American Association for the Advancement of Science)

Topics: Covalent organic framework, Pyrene and Band gap

Related papers:

- [Porous, Crystalline, Covalent Organic Frameworks](#)
- [The atom, the molecule, and the covalent organic framework](#)
- [Covalent organic frameworks \(COFs\): from design to applications](#)
- [Covalent organic frameworks: a materials platform for structural and functional designs](#)
- [Covalent organic frameworks](#)

Share this paper:    

View more about this paper here: <https://typeset.io/papers/two-dimensional-sp2-carbon-conjugated-covalent-organic-mget6nyze1>

Two-Dimensional sp^2 -Carbon-Conjugated Covalent Organic Frameworks

Enquan Jin,¹ Mizue Asada,² Qing Xu,¹ Sasanka Dalapati,¹ Matthew A. Addicoat,³ Michael A. Brady,⁴ Hong Xu,¹ Toshikazu Nakamura,² Thomas Heine,⁵ Qihong Chen¹ & Donglin Jiang^{1*}

Affiliations:

¹Field of Energy and Environment, School of Materials Science, Japan Advanced Institute of Science and Technology, 1-1 Asahidai, Nomi 923-1292, Japan.

²Department of Materials Molecular Science, Institute for Molecular Science, 38 Nishigo-naka, Myodaiji, Okazaki 444-8585, Japan.

³School of Science and Technology, Nottingham Trent University, Clifton Lane, NG11 8NS, UK.

⁴Molecular Foundry and Advanced Light Source, Lawrence Berkeley National Laboratory, 1 Cyclotron Road, Mailstop 15R0317, Berkeley, CA 94720, USA.

⁵Wilhelm-Ostwald-Institute for Physical and Theoretical Chemistry, Leipzig University, Linnéstrasse 2, 04103 Leipzig, Germany.

*Correspondence author. E-mail: djiang@jaist.ac.jp

Abstract: We synthesized a two-dimensional (2D) crystalline covalent organic framework (sp^2 c-COF) that was designed to be fully π -conjugated and constructed from all sp^2 -carbons by C=C condensation reactions of tetrakis(4-formylphenyl)pyrene and 1,4-phenylenediacetonitrile. The C=C linkages topologically connect pyrene knots at regular intervals into a 2D lattice with π -conjugations extended along both x and y directions, and develop an eclipsed layer framework rather than the more conventionally obtained disordered structures. The sp^2 c-COF is a semiconductor with a discrete band gap of 1.9 eV and can be chemically oxidized to enhance conductivity by 12 orders of magnitude. The generated radicals are confined on the pyrene knots, enabling the formation of a paramagnetic carbon structure with high spin density. The sp^2 -carbon framework induces ferromagnetic phase transition to develop spin-spin coherence and align spins unidirectionally across the material.

One Sentence Summary: A 2D sp^2 -carbon framework is synthesized being fully π -conjugated to attain exceptional spin density and is capable of unidirectional spin alignment.

Main Text: Covalent organic frameworks that exploit conjugated bonding based on sp^2 -hybridized carbons could create materials with exceptional electronic and magnetic properties (1). To design such an extended structure, the sp^2 -carbon chains must be able to diverge at regular intervals. Such branches should have appropriate geometry for extended π -conjugation at the point of knot, so that the chains strictly propagate along the x and y directions without blocking the extension of π -conjugation. However, amorphous materials will form if the sp^2 -carbon bond formation reactions are irreversible if an in-situ structural self-healing process is lacking (2, 3). Thus, designing well-defined 2D materials and fabricating extended sp^2 -carbon networks with chain propagation along both x and y directions are challenging goals.

We report a topology-directed reticular construction of crystalline sp^2 -carbon-conjugated covalent organic framework (sp^2 c-COF) by designing a C=C bond formation reaction (Fig. 1A). This reaction (4, 5, 6, 7) enables structural self-healing under thermodynamic control during

polycondensation. Topology-directed polycondensation (8, 9, 10, 11, 12, 13) of C_2 -symmetric 1,3,6,8-tetrakis(4-formylphenyl)pyrene (TFPPy) as knots and C_2 -symmetric linear 1,4-phenylenediacetonitrile (PDAN) as linkers under solvothermal conditions (mesitylene/dioxane = 1/5 v/v, 4 M NaOH, three days, 90 °C) yielded sp^2 c-COF. The 2D sp^2 -carbon sheet consists of sp^2 -carbon chains extended along x and y directions in which pyrene units serve as interweaving registry points that are periodically pitched at 2-nm intervals (Fig. 1B and 1D). The 2D sheets crystallize and form stacked layers at 3.58 Å separation, creating ordered pyrene columnar arrays and 1D nanochannels (Fig. 1C and 1E). We use the term π -conjugation rather than 2D for sp^2 c-COF because it offers π -conjugation along both x and y directions. Note that a 2D sheet can form, with restricted π -conjugation blocked at the point of vertices, as occurs in 2DPPV (two-dimensional polyphenylenevinylene framework) knotted by all *meta*-substituted 1,3,5-phenyl focal units (14). We unexpectedly found that the fully conjugated 2D layers offer the structural base of an sp^2 -carbon lattice that can accommodate exceptionally dense spins and unidirectional spin alignment via ferromagnetic phase transition.

The chemical structure of sp^2 c-COF was characterized by various analytical methods [see supplementary materials, figs. S1 to S7, and tables S1 and S2 (15)]. Fourier-transform infrared spectroscopy revealed that the peak at 2220 cm^{-1} was newly appeared for the cyano side group (16) and the peak at 2720 cm^{-1} assigned to the C–H bond of the aldehyde group was greatly attenuated, indicating the polycondensation between TFPPy and PDAN (fig. S1). Solid-state ^{13}C nuclear magnetic resonance spectroscopy of sp^2 c-COF revealed that the peak at 24.20 ppm for methylene carbon of PDAN disappeared upon polycondensation and the peak at 120.44 ppm assigned to PDAN units was shifted to 107.74 ppm (cyano side group), indicating the formation of C=C linkages in sp^2 c-COF (fig. S2). Similar spectral changes were also observed for a model compound (a TFPPy core bound to four PDAN groups) (figs. S1 and S2, scheme S1A). Field-emission scanning electron microscopy revealed that sp^2 c-COF and model compound adopted a belt morphology (fig. S3). Thermogravimetric analysis suggested that sp^2 c-COF was stable up to 350°C under nitrogen (fig. S4).

The sp^2 c-COF exhibited powder x-ray diffraction (PXRD) peaks at 3.6°, 5.2°, 5.9°, 7.3°, 11.2°, 11.8°, 14.2°, and 24.7°, which were assigned to the (110), (200), (210), (220), (240), (420), (520) and (001) facets, respectively (fig. S5, red curve and inset). We optimized the conformation of 2D single layer and the configuration of different stacking models using density functional theory tight binding calculations (17, 18). The energetically most favorable AA-stacking model yielded a PXRD pattern (fig. S5, pink curve) in good agreement with the experimentally observed profile. The Pawley-refined PXRD pattern (fig. S5, black curve) with the $C2/m$ space group with unit-cell parameters of $a = 34.4632$ Å, $b = 35.4951$ Å, $c = 3.7199$ Å, $\alpha = \gamma = 90^\circ$ and $\beta = 104.0277^\circ$ reproduced the experimentally observed curve with negligible differences (fig. S5, green curve). Tables S1 and S2 summarize the atomistic coordinates generated by DFTB calculation and Pawley refinements, respectively. Thus, the reconstruction of sp^2 c-COF structure shows an extended 2D tetragon lattice with sp^2 -carbon backbones along x and y directions (Fig. 2A). The presence of the (001) facet at 24.7° suggests the structural ordering with 3.58 Å separation in the z direction perpendicular to the 2D sheets (Fig. 2B).

The sp^2 c-COF exhibited reversible nitrogen sorption isotherm curves with a Brunauer-Emmett-Teller (BET) surface area of 692 $\text{m}^2 \text{g}^{-1}$ (fig. S6A). The pore size distribution profile revealed that sp^2 c-COF is microporous with pore size of 1.88 nm (fig. S6B). This result is consistent with the lattice as revealed by the structural analysis.

Solid-state electronic absorption spectroscopy of sp^2c -COF (fig. S7A, red curve) showed an absorption band at 498 nm, whose red-shift of 53-nm from that of the model compound (fig. S7A, black curve, scheme S1A) is indicative of extended π -conjugation. In contrast, the imine-linked 2D COF (fig. S7A, blue curve, figs. S8 and S9, scheme S1B), an analog to sp^2c -COF, exhibited an absorption band blue-shifted 21-nm relative to sp^2c -COF, indicating that the C=C linkage is more effective in transmission of π -conjugation over the 2D lattice than that of the C=N bond. Moreover, the contrast in the optical colors (fig. S7B) between sp^2c -COF (red), imine-linked 2D COF (yellow) and model compound (yellow-orange) also reflects the extended π -conjugation in sp^2c -COF. Cyclic voltammetry of sp^2c -COF (fig. S10) revealed an oxidation potential at 0.94 V and reduction potential at -0.96 V, indicating a narrow band gap of 1.90 eV. The highest occupied molecular orbital (HOMO) level was evaluated (I_9) as -5.74 eV and the lowest unoccupied molecular orbital (LUMO) level was -3.84 eV, constituting a semiconductor band structure.

The sp^2c -COF solid samples were chemically oxidized by iodine and pressed to make thin discs with a thickness of 0.08 cm. The electrical conductivity was measured across a 0.2-cm-width Pt gap electrode under air at 25 °C. The iodine-doped sp^2c -COF exhibited a linear current-voltage (I - V) profile indicative of ohmic conduction (fig. S11, red curve). The slope gave a conductivity of 7.1×10^{-2} S m^{-1} . The pristine COF sample was an insulator with a conductivity of only 6.1×10^{-14} S m^{-1} (fig. S11, black curve).

To investigate the feature of radical species in the 2D sp^2 -carbon framework, we monitored the doping process of the COF samples in the presence of iodine vapor under iodine-saturated pressure in a sealed quartz tube with electron spin resonance spectroscopy (ESR, Fig. 3). An ESR signal appeared at $g = 2.003$, just after 3-min iodine doping (Fig. 3A). The peak-to-peak height increased and leveled off after 1 day doping (Fig. 3B). The increase in ESR intensity with iodine doping indicates that the charge carriers generated also possess a spin degree of freedom. The ESR linewidth and resonance field (g -factor) were almost constant regardless of the doping level; the shift of the g -factor from that of free electron ($g = 2.0023$) was very small. The ESR linewidth of 0.13 mT indicates that the sp^2 -carbon lattice is free of anisotropic g -tensor and hyperfine interactions. These results suggest that the frontier electrons maintain to locate at the pyrene knots and do not form non-radical bipolarons.

The temperature dependence of the spin susceptibility χ_{spin} determined by integrating the ESR signal intensity (Fig. 3C) shows that the g -factor was temperature independent. The Curie-like enhancement of the χ_{spin} value indicates the existing spin freedom persists to the low temperature (Fig. 3C). Figure 3D shows the temperature dependency of the ESR linewidth ΔH_{pp} . The ESR linewidth is almost constant above 100 K. The temperature independent ESR linewidth is dominated by the spin-spin exchange interaction through space between spins in neighboring layers and indicates the localized nature of the spins at the pyrene knots. Considerable exchange interaction between spins is an evidence for the high density of spins generated in the iodine-doped sp^2c -COF. The ESR linewidth gradually increased below 100 K, suggesting that long-range magnetic order developed in the framework. Such a 2D spin structure is inaccessible by either 1D conjugated polymers (20, 21) or conventional 2D COFs (1).

The absence of bipolarons observed for sp^2c -COF is totally different from 1D conjugated polymers, which eventually form bipolarons without spins and greatly diminish the spins in the doped materials (22, 23, 24, 25). We compared the ESR spectra with those of 1D sp^2c -polymer (scheme S2) and C=N linked 2D COF upon iodine doping, which gave rise to only very weak ESR signals (fig. S12). Indeed, the ESR intensity of sp^2c -COF was 120 and 25 fold higher than

those of 1D sp^2c -polymer and C=N linked 2D COF at room temperature, respectively. The fully π -conjugated sp^2c -carbon 2D lattice is essential for generating high-density radicals in the materials. Moreover, we investigated the structure of crystalline sp^2c -COF upon iodine doping using wide-angle x-ray scattering (WAXS) (26, 27). The WAXS peaks were unchanged before and after prolonged iodine doping with respect to the (110), (200), (210), (220), (240), (420) and (001) facets (fig. S13), indicating that the pyrene arrays retain upon chemical oxidation.

To verify the observed long-range order was intrinsic, we performed magnetic susceptibility measurements using SQUID (superconducting quantum interference device) magnetometry. Figure 4A shows the temperature dependence of the magnetic susceptibility (χ). The spin susceptibility determined by both ESR and SQUID measurements were in agreement in the entire temperature range. Above 100 K, the spins were paramagnetic and randomly oriented in the material. Remarkably, the magnetic susceptibility was greatly enhanced below 100 K. By using the magnetic susceptibility below 30 K and assuming $S = 1/2$ spin, the spin concentration and the Weiss temperature Θ was estimated to be 0.7 per pyrene unit and 8.1 K, respectively. Therefore, iodine-doped sp^2c -COF with exceptionally dense spins is a bulk magnet.

Magnetization (M)-applied field (H) relations revealed that sp^2c -COF yielded linear curves at the temperatures above 20 K; below 10 K, the M-H plots became nonlinear (Fig. 4B, blue and red curves). The nonlinearity denotes a ferromagnetic phase transition, whereas the spin-spin coherence is developed with unidirectionally aligned spins across the material (Fig. 4C).

As controls, we investigated the electronic and magnetic behaviors of the model compound, a 1,6-linear polymer (scheme S3) and an amorphous version of sp^2c -COF named as sp^2c -CMP (scheme S4), which has the same building units as sp^2c -COF but it does not possess ordered layer structure (figs. S14A to C). The 1,6-linear polymer exhibited an absorption band at 446 nm (fig. S15) and electronic bandgap of 2.34 eV (fig. S16B, table S3). The sp^2c -CMP sample exhibited an adsorption band at 436 nm (fig. S15), which is 62-nm blue-shifted from that of sp^2c -COF (498 nm). From the adsorption spectrum, the optical bandgap of sp^2c -CMP was evaluated to be 2.01 eV, whereas its electronic bandgap was 1.96 eV (fig. S16C, table S3) according to the CV measurements. Upon doping with iodine, the model compound exhibited a conductivity of only $4.1 \times 10^{-8} \text{ S m}^{-1}$ (fig. S17A) and an ESR intensity of 1/100 that of sp^2c -COF (figs. S18A and B). The spin density is negligible (figs. S19A and B). The model compound upon doping did not exhibit magnetic state transition and magnetic field response from the M-H curve (fig. S20A). The 1,6-linear polymer upon doping with iodine exhibited a conductivity of $2.9 \times 10^{-7} \text{ S m}^{-1}$ (fig. S17B). From the time-dependent ESR measurements (fig. S18C), the saturated ESR intensity is 1/406 that of sp^2c -COF (fig. S18A). The 1,6-linear polymer had a spin density of only 0.004 per pyrene unit (figs. S19A and C) and did not exhibit magnetic state transition and magnetic field response (fig. S20B). The sp^2c -CMP samples upon doping with iodine exhibited a conductivity of $8.1 \times 10^{-3} \text{ S m}^{-1}$ (fig. S17C), which is one order of magnitude lower than that of sp^2c -COF. The time-dependent ESR measurements revealed signals at $g = 2.003$ (fig. S18D). However, the saturated ESR intensity is only 1/5 that of sp^2c -COF (fig. S18A). Indeed, the spin density is 0.057 per pyrene unit (figs. S19A and D). These results that the amorphous sp^2c -CMP cannot form a dense spin system. The SQUID measurements revealed that a small amount of part of sp^2c -CMP is paramagnetic at room temperature and shows trace of superparamagnetic at low temperature (fig. S20C, $\Theta = 1.5 \text{ K}$), as indicated by the decreased magnetism after the field of 40000 Oe (red curve). In contrast, the ferromagnetism with increasing magnetism is an overwhelming majority in sp^2c -COF with saturated magnetism after

the field of 40000 Oe (Fig. 4B, red curve). These results confirmed that the observed electronic and spin functions are inherent to sp^2 -c-COF and originate from its extended crystalline structure.

References and Notes:

1. N. Huang, P. Wang, D. Jiang, Covalent organic frameworks: a materials platform for structural and functional designs. *Nat. Rev. Mater.* **1**, 16068 (2016). doi: 10.1038/natrevmat2016.68.
2. Y. Xu, S. Jin, H. Xu, A. Nagai, D. Jiang, Conjugated microporous polymers: design, synthesis and application. *Chem. Soc. Rev.* **42**, 8012-8031 (2013).
3. J.-X. Jiang, F. Su, A. Trewin, C. D. Wood, N. L. Campbell, H. Niu, C. Dickinson, A. Y. Ganin, M. J. Rosseinsky, Y. Z. Khimiyak, A. I. Cooper, Conjugated microporous poly(aryleneethynylene) networks. *Angew. Chem. Int. Ed.* **46**, 8574-8578 (2007).
4. D. T. Mowry, The knoevenagel condensation of aryl alkyl ketones with malononitrile. *J. Am. Chem. Soc.* **67**, 1050-1051 (1945).
5. H. E. Zimmerman, L. Ahramjian, Overlap control of carbanionoid reactions. II. The stereochemistry of the perkin reaction and related condensation reactions. *J. Am. Chem. Soc.* **81**, 2086-2091 (1959).
6. S. Patai, Y. Israeli, The kinetics and mechanisms of carbonyl-methylene condensations. Part VII. The reaction of malononitrile with aromatic aldehydes in ethanol. *J. Chem. Soc.* 2025-2030 (1960).
7. D. A. M. Egbe, T. Kietzke, B. Carbonnier, D. Mühlbacher, H.-H. Hörhold, D. Neher, T. Pakula, Synthesis, characterization, and photophysical, electrochemical, electroluminescent, and photovoltaic properties of Yne-containing CN-PPVs. *Macromolecules* **37**, 8863-8873 (2004).
8. P. J. Waller, F. Gandara, O. M. Yaghi, Chemistry of covalent organic frameworks. *Acc. Chem. Res.* **48**, 3053-3063 (2015).
9. J. W. Colson, A. R. Woll, A. Mukherjee, M. P. Levendorf, E. L. Spitler, V. B. Shields, M. G. Spencer, J. Park, W. R. Dichtel, Oriented 2D covalent organic framework thin films on single-layer graphene. *Science* **332**, 228-231 (2011).
10. L. Ascherl, T. Sick, J. T. Margraf, S. H. Lapidus, M. Calik, C. Hettstedt, K. Karaghiosoff, M. Döblinger, T. Clark, K. W. Chapman, F. Auras, T. Bein, Molecular docking sites designed for the generation of highly crystalline covalent organic frameworks. *Nat. Chem.* **8**, 310-316 (2016).
11. S. Kandambeth, A. Mallick, B. Lukose, M. V. Mane, T. Heine, R. Banerjee, Construction of crystalline 2D covalent organic frameworks with remarkable chemical (acid/base) stability via a combined reversible and irreversible Route. *J. Am. Chem. Soc.* **134**, 19524-19527 (2012).
12. M. R. Rao, Y. Fang, S. De Feyter, D. F. Perepichka, Conjugated covalent organic frameworks via michael addition-elimination. *J. Am. Chem. Soc.* **139**, 2421-2427 (2017).
13. X.-H. Liu, C.-Z. Guan, S.-Y. Ding, W. Wang, H.-J. Yan, D. Wang, L.-J. Wan, On-surface

- synthesis of single-layered two-dimensional covalent organic frameworks via solid–vapor interface reactions. *J. Am. Chem. Soc.* **135**, 10470-10474 (2013).
14. X. Zhuang, W. Zhao, F. Zhang, Y. Cao, F. Liu, S. Bi, X. Feng, A two-dimensional conjugated polymer framework with fully sp^2 -bonded carbon skeleton. *Polym. Chem.* **7**, 4176-4181 (2016).
 15. Materials and methods, figs. S1-S7 and tables S1 and S2 are available as supplementary materials on Science Online.
 16. B. C. Thompson, Y.-G. Kim, T. D. McCarley, J. R. Reynolds, Soluble narrow band gap and blue propylenedioxythiophene-cyanovinylene polymers as multifunctional materials for photovoltaic and electrochromic applications. *J. Am. Chem. Soc.* **128**, 12714-12725 (2006).
 17. B. Aradi, B. Hourahine, T. Frauenheim, DFTB+, a sparse matrix-based implementation of the DFTB method. *J. Phys. Chem. A* **111**, 5678-5684 (2007).
 18. <http://www.dftb.org>
 19. HOMO = $-e(E_{\text{oxidation, onset}} + 4.8 - E_{\text{Fc/Fc}^+})$; LUMO = $-e(E_{\text{reduction, onset}} + 4.8 - E_{\text{Fc/Fc}^+})$
 20. J. L. Bredas, G. B. Street, Polarons, bipolarons and solitons in conducting polymers. *Acc. Chem. Res.* **18**, 309-315 (1985).
 21. S. Kuroda, K. Marumoto, Y. Shimoi, S. Abe, ESR spectroscopy of polarons in conjugated electroluminescent polymers. *Thin Solid Films* **393**, 304-309 (2001).
 22. A. Sakamoto, Y. Furukawa, M. Tasumi, Resonance raman and ultraviolet to infrared absorption studies of positive polarons and bipolarons in sulfuric-acid-treated poly(*p*-phenylenevinylene). *J. Phys. Chem.* **98**, 4635-4640 (1994).
 23. I. Orion, J. P. Buisson, S. Lefrant, Spectroscopic studies of polaronic and bipolaronic species in *n*-doped poly(paraphenylenevinylene). *Phys. Rev. B* **57**, 7050-7065 (1998).
 24. W. R. Salaneck, R. H. Friend, J. L. Brédas, Electronic structure of conjugated polymers: consequences of electron–lattice coupling. *Phys. Rep.* **319**, 231-251 (1999).
 25. R. R. Chance, J. Bredas, R. Silbey, Bipolaron transport in doped conjugated polymers. *Phys. Rev. B* **29**, 4491 (1984).
 26. A. Hexemer, W. Bras, J. Glossinger, E. Schaible, E. Gann, R. Kirian, A. MacDowell, M. Church, B. Rude, H. Padmore, A SAXS/WAXS/GISAXS beamline with multilayer monochromator. *J. Phys. Conf. Ser.* **247**, 012007 (2010).
 27. J. Ilavsky, Nika: software for two-dimensional data reduction. *J. Appl. Cryst.* **45**, 324-328 (2012).
 28. S. S. P. Parkin, J. C. Scott, J. B. Torrance, E. M. Engler, Antiferromagnetic resonance in tetramethyltetrathiafulvalene bromide [(TMTTF)₂Br]. *Phys. Rev. B* **26**, 6319-6321 (1982).
 29. G. A. Bain, J. F. Berry, Diamagnetic corrections and Pascal's constants. *J. Chem. Educ.* **85**, 532-536 (2008).
 30. S. Dalapati, S. B. Jin, J. Gao, Y. H. Xu, A. Nagai, D. L. Jiang, An azine-linked covalent organic framework. *J. Am. Chem. Soc.* **135**, 17310-17313 (2013).

31. M. G. Rabbani, A. K. Sekizkardes, Z. Kahveci, T. E. Reich, R. Ding, H. M. El-Kaderi, A 2D mesoporous imine-linked covalent organic framework for high pressure gas storage applications. *Chem. Eur. J.* **19**, 3324-3328 (2013).

Acknowledgments: E.J. acknowledges Chinese Scholarship Concert for financial support for his study in Japan. S.D. is now international research fellow of the Japan Society for the Promotion of Science (JSPS). M.B. acknowledges The Advanced Light Source that is supported by the Director, Office of Science, Office of Basic Energy Sciences, of the U.S. Department of Energy under Contract No. DE-AC02-05CH11231. T.H. and M.A. acknowledge supercomputer time at ZIH Dresden and financial support by the European Research Council (ERC-StG 256962 C3ENV) and the VolkswagenStiftung. D.J. acknowledge the Grant-in-Aid for Scientific Research (A) (17H01218) from MEXT, Japan, and support by ENEOS Hydrogen Trust Fund and Ogasawara Foundation for Promotion of Science and Engineering.

D.J. conceived and designed the project. E.J., Q.X., S.D., H. X. and Q.C. conducted the experiments. M.A.A. and T.H. conducted DFTB calculations and structure simulations. M.A. and T.N. conducted ESR and SQUID measurements. D.J., E.J., Q.C. and S.D. wrote the manuscript and discussed the results with the authors. All data are reported in the main text and supplement.

Figure Captions

Fig. 1. Chemical and lattice structures of a crystalline porous sp^2 -carbon framework.

(A) Schematic representation of the synthesis of the crystalline porous sp^2 -hybridized carbon covalent organic framework (sp^2 c-COF) with pyrene knots and phenylenevinylene linkers connected by C=C bonds (one pore is shown). (B and C) Reconstructed crystal structures of (B) one layer and (C) many layers of the 2D sp^2 -hybridized carbon framework (sp^2 c-COF; 3×3 unit cell). The pyrene knots are regularly interweaved in a 2 nm pitch along the x and y directions and are stacked at an interval of 3.58 Å along the z direction via π - π interactions to form ordered pyrene knot π -arrays and 1D channels. (D and E) Ball (pyrene knot) and stick (phenylenevinylene chain) representations of (D) a 2D sheet with extended π -conjugations along x and y directions and (E) the stacked sp^2 c-COF.

Fig. 2. Crystal structure. (A and B) Reconstructed crystal structure at top (A) and side (B) views. The 2D layers stacked at a 3.58 Å interval along the z direction.

Fig. 3. ESR studies. (A) Time evolution of the ESR spectra upon iodine doping. (B) The plot of the peak-to-peak height of the ESR signals versus doping time. The peak intensity was saturated after 26 h and did not decrease after doping. (C) Temperature dependency of the spin susceptibility χ_{spin} for the iodine-doped sp^2 c-COF. (D) Temperature dependency of the ESR linewidth (ΔH_{pp}).

Fig. 4. Magnetization and spin alignment. (A) Temperature dependence of the spin susceptibility, χ , determined by the SQUID magnetometer for the iodine-doped sp^2 c-COF. (B) Magnetic (M)–applied field (H) profiles at different temperatures (red, 2 K; blue, 5 K; purple, 10

K; brown, 20 K; green, 100 K; black, 300 K). The nonlinearity of the curves denotes the ferromagnetic phase transition. (C) Schematic of spin alignment in sp^2c -COF (3×3 lattice). Red arrows represent spins. The spins are isolated at the knots and are unidirectionally aligned across the framework via ferromagnetic phase transition to develop spin-spin coherence.

Supplementary Materials:

Materials and Methods

Figures S1-S20

Tables S1-S3

Schemes S1-S4

References and Notes (*1-31*)